Article

Duration of Hydrothermal Alteration and Mineralization of the Don Manuel Porphyry Copper System, Central Chile

Amy K. Gilmer [1,2,*], R. Stephen J. Sparks [2], Dan N. Barfod [3], Emily R. Brugge [2,4] and Ian J. Parkinson [2]

[1] U.S. Geological Survey, Denver, CO 80225, USA

[2] School of Earth Sciences, University of Bristol, Wills Memorial Building, Bristol BS8 1RJ, UK;
     steve.sparks@bristol.ac.uk (R.S.J.S.); e.brugge@nhm.ac.uk (E.R.B.); ian.parkinson@bristol.ac.uk (I.J.P.)

[3] Natural Environment Research Council Argon Isotope Facility, Scottish Universities Environmental Research
     Centre, East Kilbride G75 0QF, UK; dan.barfod@glasgow.ac.uk

[4] Department of Earth Science and Engineering, Imperial College London, and Department of Earth Sciences,
     Natural History Museum, London SW7 2AZ, UK

* Correspondence: agilmer@usgs.gov

Abstract: The Don Manuel porphyry copper system, located in the Miocene–Pliocene metallogenic belt of central Chile, contains spatially zoned alteration styles common to other porphyry copper deposits including extensive potassic alteration, propylitic alteration, localized sericite-chlorite alteration and argillic alteration but lacks pervasive hydrolytic alteration typical of some deposits. It is one of the youngest porphyry copper deposits in the Andes. Timing of mineralization and the hydrothermal system at Don Manuel are consistent with emplacement of the associated intrusions (ca. 4 and 3.6 Ma). Two molybdenite samples yielded consistent ages of 3.412 ± 0.037 and 3.425 ± 0.037 Ma. ^{40}Ar/^{39}Ar ages on hydrothermal biotites (3.57 ± 0.02, 3.51 ± 0.02, 3.41 ± 0.01, and 3.37 ± 0.01 Ma) are associated with potassic alteration. These ages are younger than the youngest intrusion by ~300 k.y. recording the cooling of the system below 350 °C. Such a time gap can be explained by fluxing of hot magmatic fluids from deeper magmatic sources.

1. Introduction

The temporal and spatial relationships between igneous activity, mineralization and associated hydrothermal alteration in porphyry copper deposits are an enduring topic of research. Modern geochronology provides an increasingly powerful approach to unravelling these relationships and can place time constraints on the longevity of these systems.

Here we investigate the Don Manuel igneous complex and porphyry copper system located within the Andean Cordillera of central Chile. Don Manuel is part of the Miocene–Pliocene metallogenic belt (Figure 1) and is one of the youngest porphyry copper systems in the Andes [1]. We combine geochronologic data with observations of the hydrothermal alteration, veining and mineralization in the Don Manuel porphyry copper system. Timing of mineralization and duration of hydrothermal alteration are integrated within the overall geochronological framework of magmatic activity. Finally, the Don Manuel porphyry copper system is compared with other porphyry copper deposits of the Miocene–Pliocene porphyry copper belt of central Chile. Implications for the preservation potential of porphyry copper systems in this segment of the Andes are also discussed.
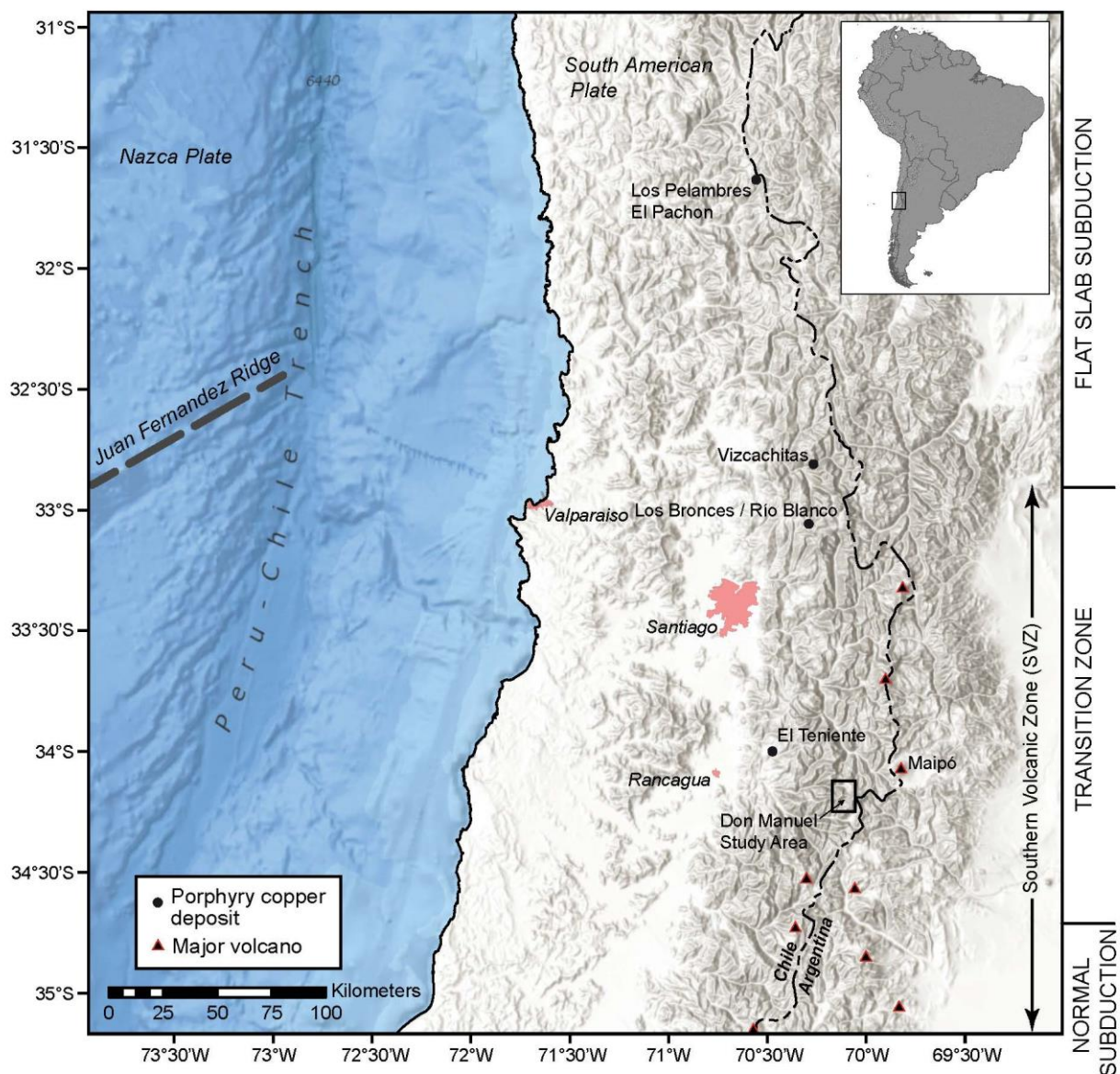
Figure 1. Location of the Don Manuel porphyry copper system, major volcanoes, and Miocene–Pliocene porphyry copper deposits (PCDs) in central Chile including El Teniente, Los Bronces-Río Blanco, Vizcachitas, and Los Pelambres.

2. Geology of the Don Manuel Porphyry Copper System

The Don Manuel study area is within the Northern Southern Volcanic Zone (NSVZ) of the Andes, approximately 25 km east of the giant porphyry copper molybdenum deposit El Teniente and 20 km from the active volcanic arc in the Principal Cordillera of the Andes (Figure 1). The Don Manuel system is located just south of the Chilean–Pampean flat slab segment [2–4], where the Nazca plate is subducting at an angle of ~10° below the South American plate [4–8].

The central Chile Miocene–Pliocene metallogenic belt includes the El Teniente, Los Bronce-Río Blanco, and Los Pelambres-El Pachón deposits [9–11]. These deposits are roughly aligned N–S in the central part of Western Principal Cordillera of the Andes, whereas Don Manuel lies farther east in the Eastern Principal Cordillera (Figure 1). The deposits in this belt typically consist of multiphase, porphyritic intrusions and related late magmatic-hydrothermal breccias [2,12] that are associated with subduction-related, calc-alkaline magmatism.

The Don Manuel study area consists of the Paredones area in the north and the Don Manuel Principal area to the south (Figure 2). Exploration in the Don Manuel area began in 2006 with reconnaissance mapping at a 1:25,000 scale carried out by Minera Aurex, a Freeport-McMoran subsidiary. Minera Aurex drilled eight holes in the southern area with reconnaissance mapping and sampling in the Paredones area [13]. BHP acquired the project area in 2010 and carried out additional sampling and reconnaissance mapping. Gilmer et al. [1] presented the first characterization of the Don Manuel igneous complex (DMIC) associated with the porphyry copper system. The Eocene to Oligocene Coya Machalí Formation hosts the DMIC and associated porphyry-style mineralization.
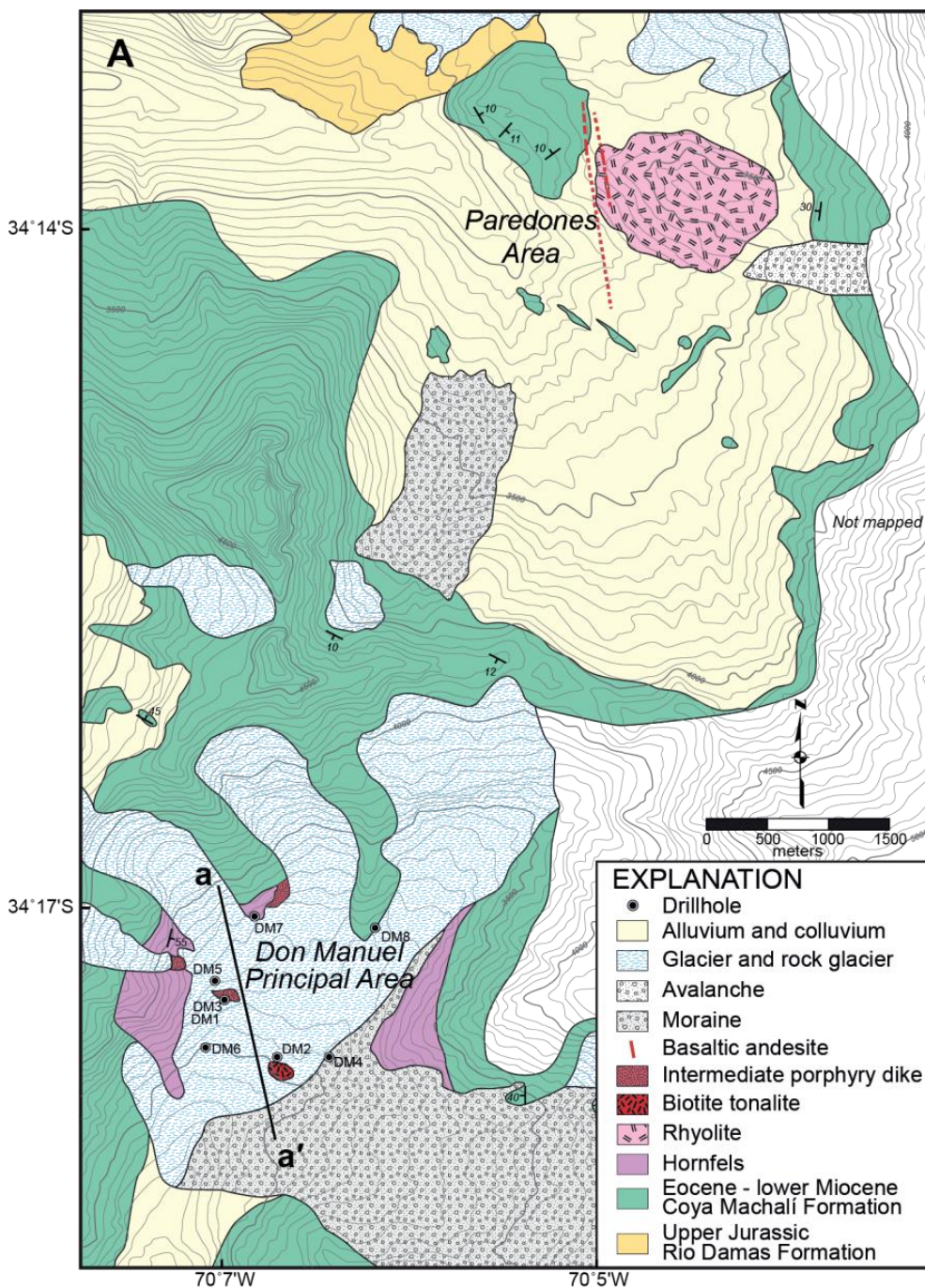

Figure 2. *Cont.*
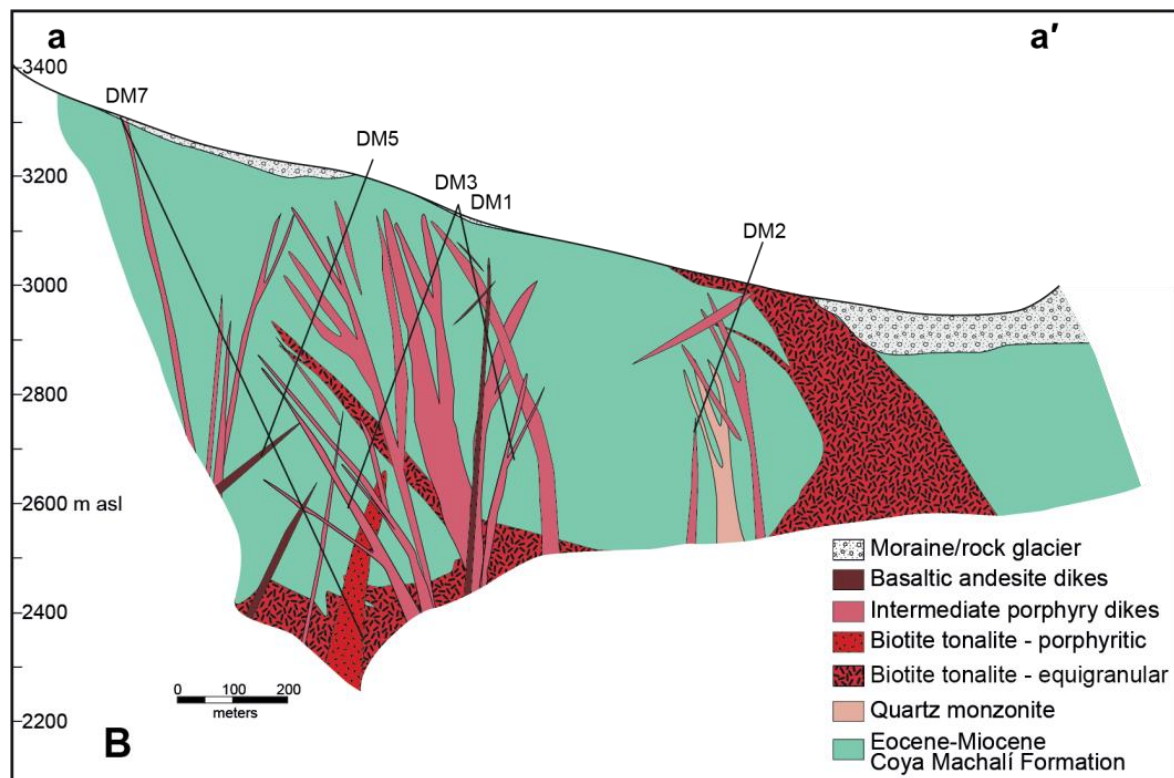
Figure 2. (**A**) Geologic map of the Don Manuel area showing the location of the Paredones and Don Manuel Principal sections of the study area and drill hole locations. Mineralization is confined to the Don Manuel Principal area. Modified after Candia et al. (2009). (**B**) Schematic cross section through the mineralized area at Don Manuel Principal. Crosscutting relationships are shown based on logging by the lead author, supplemented by logs of surface samples and drill cores from BHP.

2.1. Intrusive Rocks

The igneous units in the Don Manuel Principal area consist of quartz monzonite and biotite tonalite which are intruded by intermediate porphyritic and basaltic andesite dikes. In the Paredones area, a porphyritic rhyolite stock crops out at the surface and is crosscut by basaltic andesite dikes (Figure 2B). The DMIC magmas have undergone polybaric differentiation and show conspicuous evidence for magma mixing [1,14]. They were episodically emplaced between ca. 4 and 3.6 Ma. Chemical abrasion isotope-dilution thermal ionization mass spectrometry (CA-ID-TIMS) U-Pb zircon dates and $^{40}Ar/^{39}Ar$ whole rock ages are summarized in Table 1. The age data are consistent with the order of intrusion based on crosscutting relationships observed in cores and in the field. Previous work demonstrated episodic emplacement of the hypabyssal intrusive suite sourced from deeper pluton-scale magmatic systems [1,14]. Intrusion emplacement developed over approximately 400 k.y. with dominantly silicic but barren intrusions in the first 200 k.y., followed by emplacement of two biotite tonalite intrusions and then by multiple dikes of intermediate and mafic magmas. The most intense mineralization is temporarily and spatially associated with the emplacement of the biotite tonalities and intermediate porphyry dikes. Based on the Al-in-hornblende barometry pressures of ~1.2 kbar calculated for the biotite tonalite, the DMIC was estimated to have been emplaced at a depth of between 3.5 and 5 km [14].

In the Don Manuel Principal area, the oldest unit is the quartz monzonite, a fine- to medium-grained and locally porphyritic rock composed of plagioclase, microcline, quartz, and biotite. The quartz monzonite is cross cut by intermediate intrusions and basaltic andesite porphyry dikes. The most prominent intrusion is the biotite tonalite, which crops out at the surface, and has a minimum vertical extent of ~600 m based on drill core intersections that bottomed out in the unit (Figure 2B). The biotite tonalite consists

of an equigranular phase and a younger porphyritic phase. The equigranular biotite tonalite ranges from medium- to coarse-grained and is composed of plagioclase, biotite, microcline, quartz, and amphibole, whereas the porphyritic phase contains plagioclase, biotite, and amphibole phenocrysts. The intermediate porphyry dike (IPD) suite crosscuts the biotite tonalite. It ranges from andesite to dacite and consists of dikes with widths ranging from less than a meter to 60 m. All IPDs contain phenocrysts of plagioclase, but may have phenocrysts of either amphibole, biotite, or both. Rarely do they contain quartz phenocrysts, and where present, they are embayed. The groundmass of these dikes consists of plagioclase, amphibole, biotite, and quartz. The IPDs are in turn cut by aphanitic to porphyritic basaltic andesite dikes containing phenocrysts of plagioclase and amphibole where porphyritic and the matrix contains plagioclase, amphibole and biotite. The basaltic andesite dikes are typically less than 10 m in thickness.

Table 1. Summary of the geochronology of the Don Manuel igneous complex, Chile.

Rock Type	Location	Age
Quartz monzonite	Don Manuel Principal drill core; dikes	4.058 ± 0.015 Ma [1,3] 3.975 ± 0.058 Ma [1,3]
Rhyolite	Paredones; stock; outcrop	3.879 ± 0.018 Ma [1,3]
Biotite tonalite	Don Manuel Principal drill core; stock	3.829 ± 0.010 Ma [1,3]
Biotite tonalite (porphyritic phase)	Don Manuel Principal drill core; dikes	3.733 ± 0.010 Ma [1,3]
Intermediate porphyry dike (IPD) suite	Don Manuel Principal drill core; dikes	
Type 1		3.733 ± 0.048 Ma [1,3]
Type 2		3.657 ± 0.031 Ma [1,3] 3.656 ± 0.029 Ma [1,3]
Type 3		3.912 ± 0.057 Ma [1,3]
Mafic enclaves	Don Manuel Principal drill core; hosted by rhyodacite, biotite tonalite, and IPD	
Cpx basaltic andesite dikes	Paredones; dikes; outcrop	
Basaltic andesite dikes	Don Manuel Principal drill core; occurs as dikes	3.85 ± 0.19 Ma [2,3]; 3.36 ± 0.09 Ma [2,3]; 3.24 ± 0.06 Ma [2,3]; 2.96 ± 0.11 Ma [2,3]; 2.88 ± 0.06 Ma [2,3]

[1] CA-ID-TIMS U-Pb zircon; [2] ^{40}Ar-^{39}Ar whole rock; [3] Gilmer et al. (2017).

In the Paredones area, the oldest unit is rhyolite, which crops out at the surface as a ~1.5 km diameter subcircular, hypabyssal stock. The rhyolite is predominately porphyritic with plagioclase and biotite phenocrysts and rare quartz eyes. The rhyolite is crosscut by porphyritic basaltic andesite dikes with plagioclase, clinopyroxene, biotite, and minor amphibole phenocrysts. These dikes have not been dated.

2.2. Coya Machalí Formation

The late Oligocene-early Miocene-aged Coya Machalí Formation rocks in the study area consist of volcaniclastic deposits interbedded with fluvial and lacustrine sediments and basaltic andesitic lavas (Figure 3). This formation is equivalent to the Abanico Formation to the north [15,16] which has been interpreted to have been deposited in a north–south intra-arc basin [17]. In the Don Manuel area, the Coya Machalí Formation lithologies include porphyritic basaltic andesitic lava flows with up to 10% phenocrysts, primarily plagioclase with minor clinopyroxene. Interbedded with the basaltic andesite lava flows are volcaniclastic rocks consisting of alternating feldspathic sandstones and finely laminated mudstones (2–3 mm thick). Calcareous siltstones and calcite-cemented coarse-grained feldspar and quartz sandstones are also present in the core and crop out at the surface.
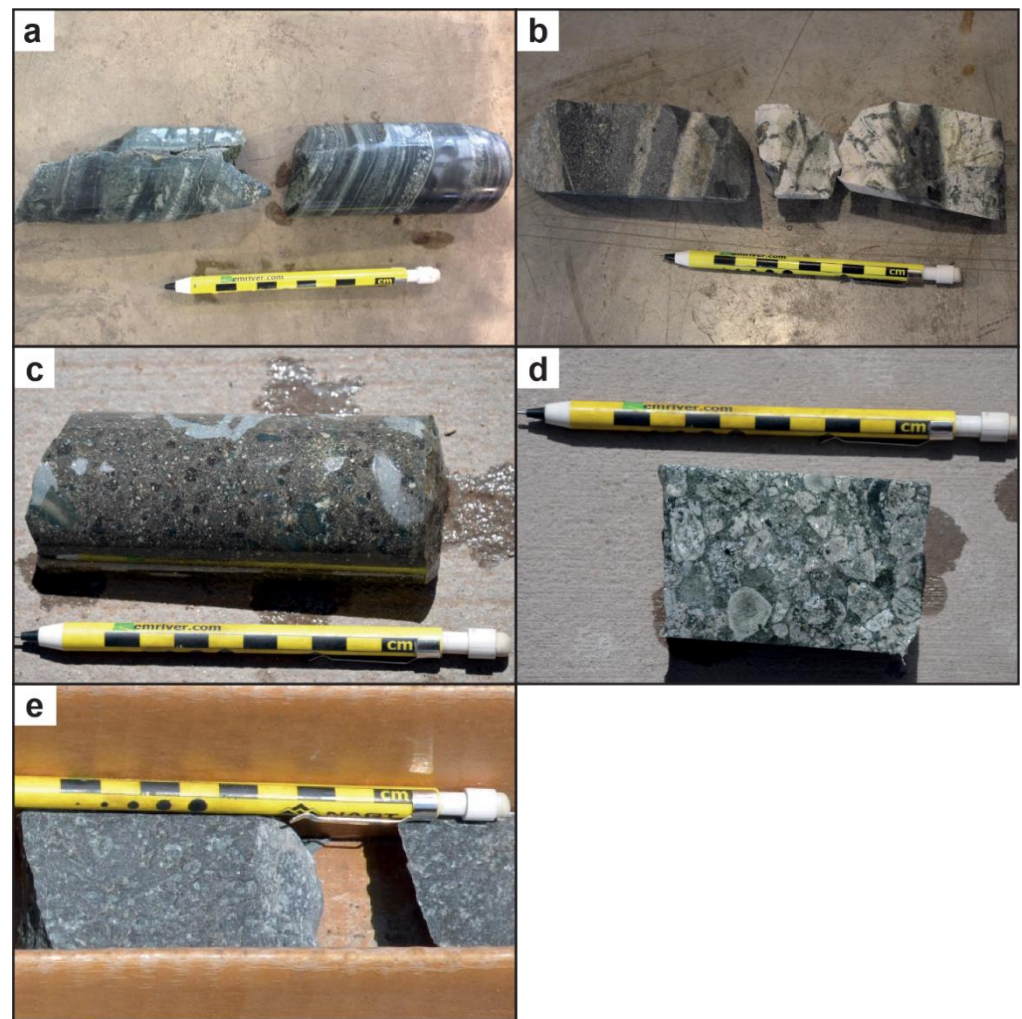
Figure 3. Variably hydrothermally altered and metamorphosed lithologies of the Coya Machalí Formation. (**a**) Finely laminated siltstone and mudstone showing chlorite and epidote alteration (DM1AG03). (**b**) Silicified siltstone and sandstone (DM1AG16). (**c**) Coarse-grained volcaniclastic sandstone (DM7AG03). (**d**) Conglomerate lithology with predominantly rounded dacitic and andesitic clasts (DM7AG07). (**e**) Propylitically altered basaltic andesite (DM7AG29).

3. Hydrothermal Alteration and Mineralization

Eight drill cores from the Don Manuel Principal area were logged and sampled to characterize and establish the timing of the alteration and mineralization. Moraines, alluvium, and glaciers cover much of the Paredones and Don Manuel Principal areas so observations were primarily restricted to drill core with some field observations and sampling in the Paredones area. Samples were examined petrographically using both transmitted and reflected light, as well as by scanning electron microscopy (SEM) at the University of Bristol (Bristol, UK).

Hydrothermal alteration in the DMIC and Coya Machalí Formation host rocks varies in intensity and is locally discontinuous. Hypogene sulfide mineralization is confined to the Don Manuel Principal area, with the Paredones area only displaying iron oxide staining. Overall, the Don Manuel porphyry copper system lacks the pervasive destructive hydrolytic alteration and dense stockwork veining commonly found in porphyry copper deposits. Hydrothermal alteration and vein types are characterized based on drill core observations, crosscutting relationships, and petrography (Table 2). Alteration stages include early silicification and calc-silicate alteration, sodic-calcic alteration, potassic alteration, propylitic alteration, sericite-chlorite alteration and argillic alteration.

Table 2. Don Manuel vein types and paragenesis.

Vein Stage	Vein Type	Subtype	Mineralogy	Vein Halo	Associated Alteration Stage
Early stage	1		Magnetite ± quartz	Biotite	Potassic/sodic-Calcic (localized)
	2		Biotite ± actinolite ± chlorite	Biotite	Potassic/sodic-Calcic (localized)
	3		Quartz ± K-feldspar, biotite, epidote, anhydrite, chalcopyrite, magnetite	Biotite ± chlorite/no halo	Potassic
Primary mineralization stage	4	a	Quartz ± K-feldspar, anhydrite, chalcopyrite, pyrite, bornite, specularite, molybdenite	No halo/K-Feldspar halo	Potassic
		b	Chalcopyrite ± quartz, pyrite	No halo/K-Feldspar halo	Potassic
	5		Chlorite + quartz ± actinolite, K-feldspar, pyrite, chalcopyrite	Quartz halo/no halo	Potassic/propyllitic
	6		Quartz + anhydrite ± chalcopyrite, pyrite, molybdenite, bornite, specularite, fluorite	No halo	Chlorite-sericite
Late mineralization stage	7		Quartz ± chalcopyrite, pyrite, specularite, molybdenite, calcite	Sericite ± chlorite halo	Chlorite-sericite
	8		Quartz + anhydrite ± carbonate, chalcopyrite, pyrite, specularite, molybdenite	Sericite ± chlorite halo	Chlorite-sericite
	9		Carbonate ± barite, gypsum, specularite, pyrite, molybdenite	Sericite halo or no halo	Argillic

3.1. Early Stage

At Don Manuel, the earliest alteration is localized and related to the emplacement of the biotite tonalite stock. Intense silicification occurs adjacent to contacts between biotite tonalite and the quartz monzonite and Coya Machalí Formation. Fine-grained quartz (<100 µm) has locally replaced the primary textures in the quartz monzonite. Within the Coya Machalí Formation, sedimentary and volcaniclastic rocks have been transformed into siliceous hornfels.

The diversity of lithologies in the Coya Machalí Formation and their variable susceptibility to alteration results in different alteration assemblages in the different protoliths (Figure 3a–e). The dominant alteration style consists of pervasive hydrothermal secondary biotite adjacent to the contact with the intrusive units and chlorite and epidote farther out from the contact with the intrusive units. In the more permeable layers, particularly in the coarser calc-silicate sediments, alteration and replacement is more extensive. Exoskarn is locally developed in calc-silicate sediments in proximity to intrusive contacts (Figure 4a–f). Skarn intervals (Figure 4c,e) are commonly confined to layers less than 2 cm thick within the finely laminated sediments but can reach up to 5 m thick. Two types of skarn were recognized: a garnet-clinopyroxene-epidote skarn and a clinopyroxene-magnetite-actinolite-epidote skarn. The dominant mineralogy is that of an anhydrous, prograde assemblage of andradite, diopside, epidote/clinozoisite, vesuvianite, and pyrite. Locally, a vein-related, retrograde assemblage of quartz, actinolite, chlorite, and epidote overprints this assemblage. Layers of calc-silicate sediment (up to 4 cm) have been replaced by abundant sulfides and oxides (up to 60%), including magnetite, chalcopyrite, cubanite, pyrrhotite, and pyrite (Figure 4c,d). This mineralization is accompanied by veins containing actinolite and celadonite. At shallower depths (200 m) in drill hole DM7, the clinopyroxene, garnet-free skarn assemblage shows a strong retrograde overprint (Figure 4e,f) where diopside, cummingtonite, and actinolite have been overprinted by chlorite and epidote with abundant pyrite and only minor chalcopyrite.
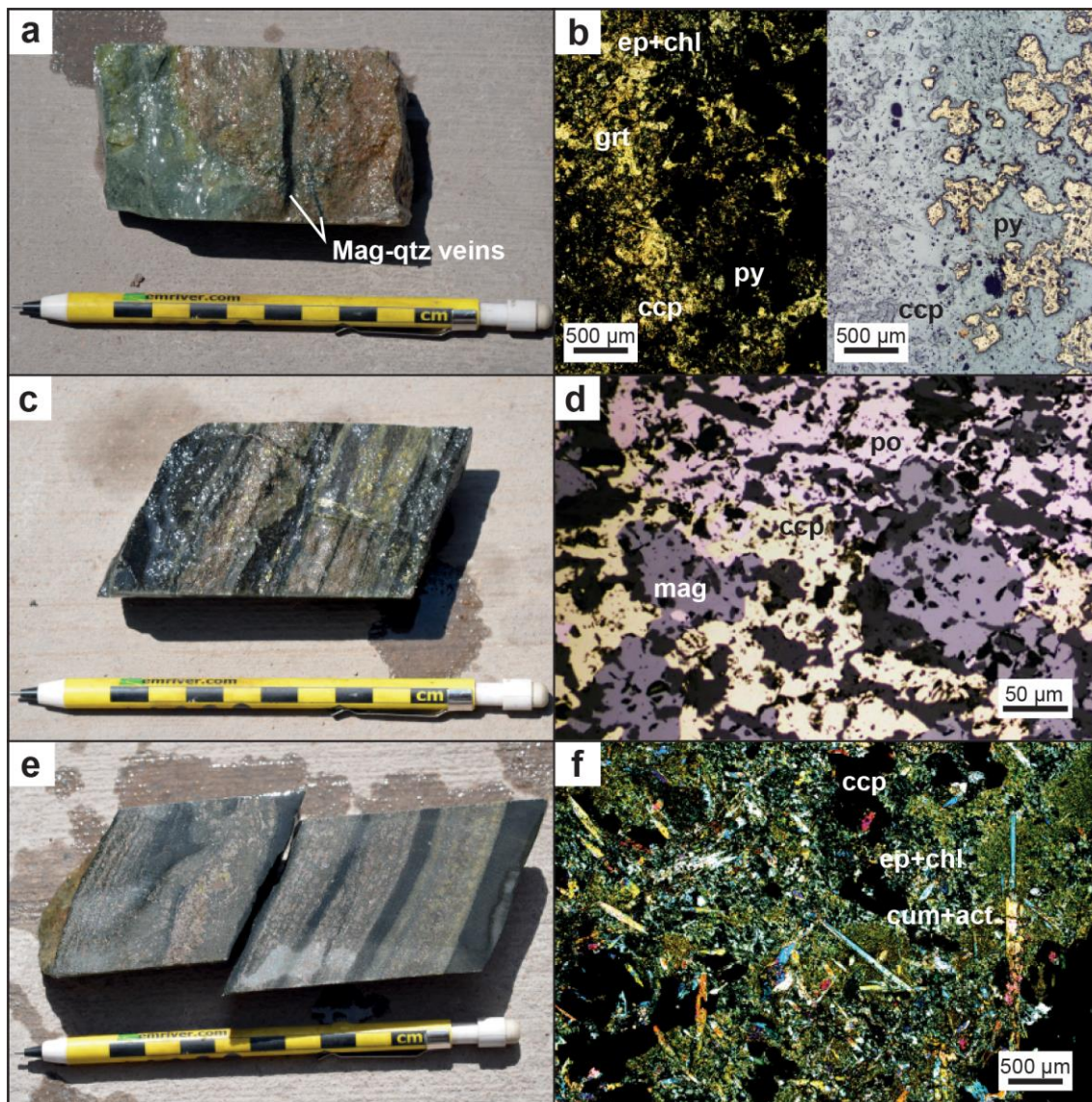
Figure 4. Examples of skarn from the Don Manuel core. (**a**) Garnet-clinopyroxene-epidote skarn from drill hole DM7, 597 m (DM7AG21). (**b**) Photomicrograph of sample DM7AG21 in plane (left) and reflected (right) light showing anhedral andradite overprinted by epidote, chlorite and chalcopyrite. (**c**) Finely layered sediments with calc-silicate layers that have been selectively altered to clinopyroxene-magnetite-actinolite-epidote skarn with some layers being replaced by abundant sulfides, DM7, 582 m (DM7AG20). (**d**) Photomicrograph of the massive sulfide layer in sample DM7AG20 in reflected light containing magnetite, chalcopyrite, and pyrrhotite. (**e**) Clinopyroxene-actinolite-epidote skarn from drill hole DM7, 201 m. (**f**) Photomicrograph of retrograde skarn assemblage with acicular cummingtonite overprinted by actinolite with fine-grained chlorite-epidote-chalcopyrite (DM7AG08) in cross-polarized light. Mineral abbreviations: act = actinolite, chl = chlorite, ccp = chalcopyrite, cum = cummingtonite, ep = epidote, grt = garnet, po = pyrrhotite, and py = pyrite. (mag = magnetite, qtz = quartz).

Early sodic-calcic alteration is confined to narrow intervals (<2 cm) in the quartz monzonite and volcaniclastics of the Coya Machalí Formation. Sodic-calcic alteration is characterized by actinolite and magnetite veinlets and vein-related albitization mostly within vein selvages (Type 1 and 2; Table 2). No sulfides were observed associated with this alteration.

These earliest alteration events were followed by potassic alteration, characterized by hydrothermal biotite and K-feldspar, magnetite and quartz, as well as abundant sulfides. Pervasive magnetite is disseminated in localized zones and as veins within the equigranular

biotite tonalite (Figures 5a and 6a) and to a lesser extent within the intermediate porphyry dikes and quartz monzonite. Magnetite-quartz veins (Type 1, Table 2) typically have diffuse and/or curvy boundaries lacking discrete contacts (Figures 5a and 6a) and many have biotite vein halos. The Coya Machalí Formation wall rocks show potassic alteration only adjacent to contacts with the biotite tonalite and intermediate porphyry dikes.
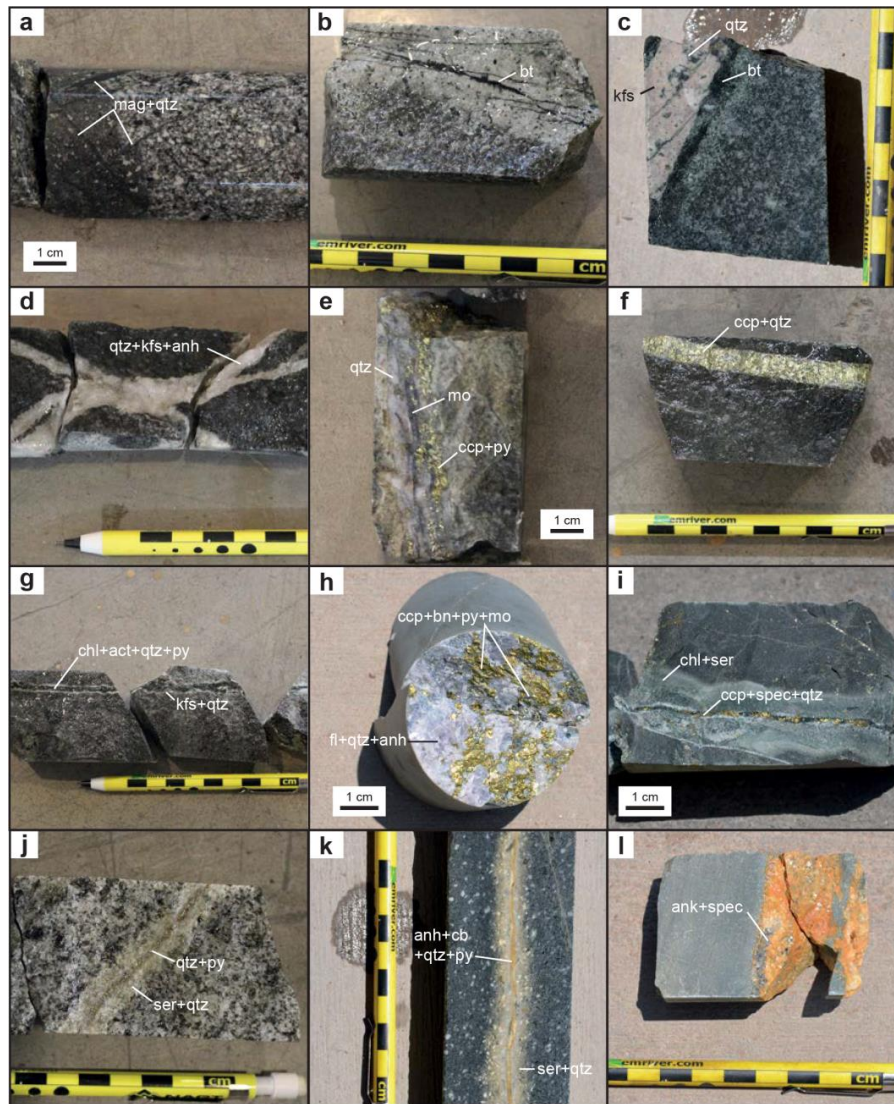

Figure 5. Examples of vein types from the Don Manuel core. (**a**) Type 1 veins containing magnetite and quartz in an IPD (DM2AG45). (**b**) Type 2 vein containing biotite in an IPD (DM8AG18). (**c**) Type 3 vein containing K-feldspar + quartz + biotite with a biotite halo in an IPD (DM8AG32). (**d**) Type 4a vein containing quartz + K-feldspar + anhydrite in an IPD (DM3AG41). (**e**) Type 4a vein containing quartz + chalcopyrite + pyrite + molybdenite in an IPD (DM8AG22). (**f**) Type 4b vein containing chalcopyrite and quartz in an IPD (DM8AG07). (**g**) Type 5 vein containing chlorite + actinolite + quartz + pyrite with a halo of quartz and K-feldspar in an IPD (DM2AG24). (**h**) Type 6 vein containing quartz + anhydrite + chalcopyrite + bornite + pyrite + molybdenite in sedimentary hornfels (DM7AG25). (**i**) Type 7 vein containing chalcopyrite + specularite + quartz with a chlorite and sericite halo in sedimentary hornfels (DM5AG05). (**j**) Type 7 vein containing quartz + pyrite with a halo of sericite and quartz in the equigranular biotite tonalite (DM2AG04). (**k**) Type 8 vein containing anhydrite + carbonate + quartz + pyrite with a sericite and quartz halo in IPD (DM6AG36). (**l**) Type 8 vein containing ankerite and specularite within sedimentary hornfels (DM7AG24). Mineral abbreviations: mag = magnetite, qtz = quartz, bt = biotite, kfs = potassium feldspar, anh = anhydrite, mo = molybdenite, ccp = chalcopyrite, py = pyrite, bn = bornite, chl = chlorite, spec = specularite, ser = sericite, cb = carbonate, and ank = ankerite.
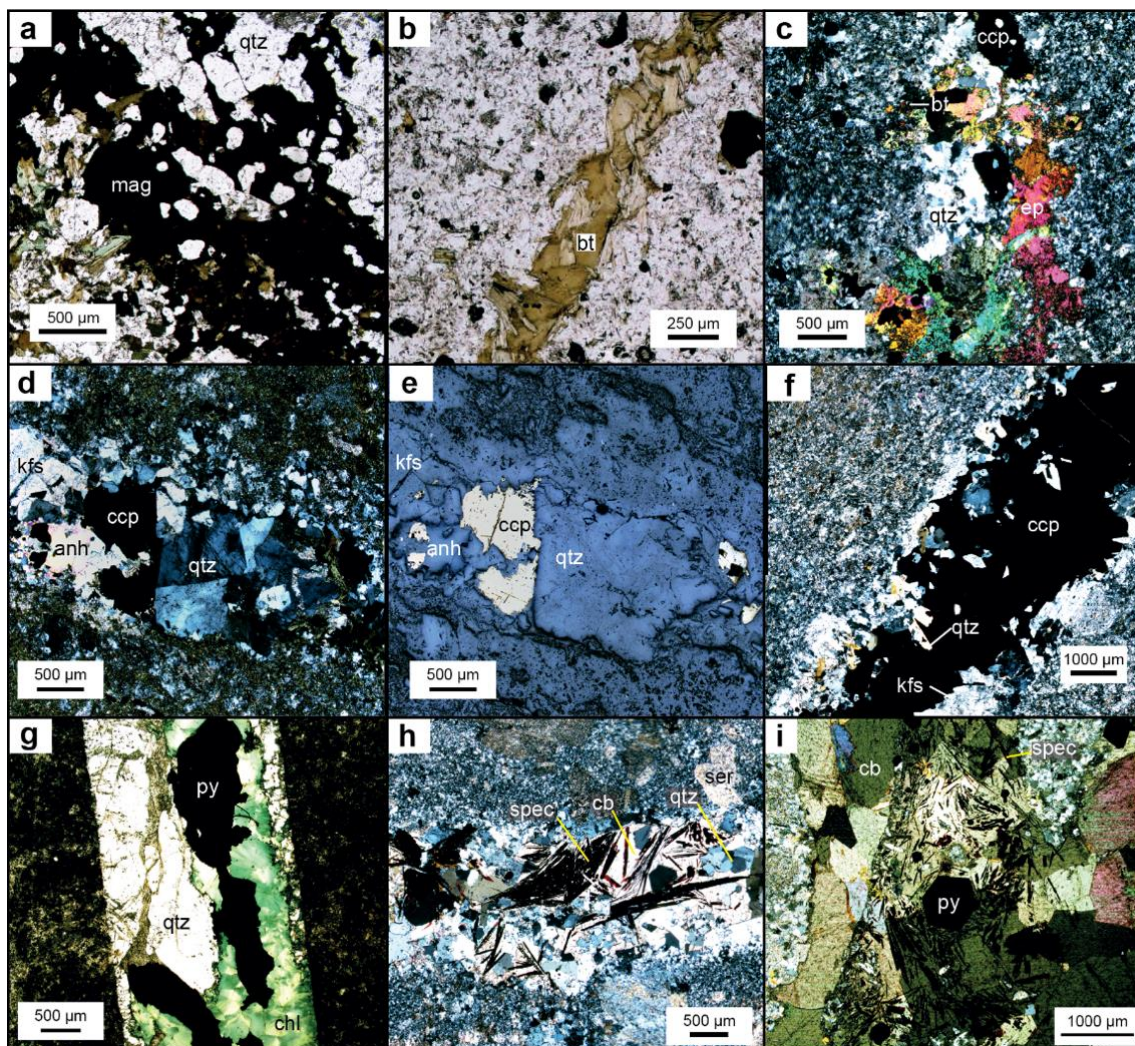
Figure 6. Photomicrographs of vein types from the core of Don Manuel. (**a**) Type 1 vein containing magnetite and quartz in an IPD (DM2AG45) in plane-polarized light. (**b**) Type 2 biotite vein in plane-polarized light in an IPD (DM2AG18). (**c**) Type 3 vein containing quartz + epidote + chalcopyrite with a weak biotite halo within an IPD (DM1AG17) in cross-polarized light. (**d**) Type 4a vein with quartz + K-feldspar + anhydrite + chalcopyrite in an IPD (DM3AG22) in cross-polarized light. (**e**) Type 4a vein previously shown in d, in reflected light. (**f**) Type 4b vein with chalcopyrite + quartz with a K-feldspar halo in an IPD in cross-polarized light. (**g**) Type 5 vein with chlorite + quartz + pyrite in an IPD in plane polarized light (DM2AG25). (**h**) Type 7 vein with quartz + calcite + specularite + pyrite with a sericite halo in an IPD in cross-polarized light. (**i**) Type 9 vein with carbonate + specularite + pyrite in a calc-silicate lithology (DM2AG13) in cross-polarized light. Mineral abbreviations: mag = magnetite, qtz = quartz, bt = biotite, ccp = chalcopyrite, ep = epidote, kfs = potassium feldspar, anh = anhydrite, py = pyrite, chl = chlorite, spec = specularite, ser = sericite, and cb = carbonate.

Hydrothermal biotite associated with potassic alteration replaces primary ferromagnesian silicates in the biotite tonalite and intermediate porphyry dikes, occurs as aggregate clots and groundmass overgrowths, and forms veins and vein selvages (Figures 5b and 6b). Amphibole phenocrysts are commonly replaced by secondary biotite while primary biotite phenocrysts are less affected. Biotite ± actinolite, chlorite veins (Type 2) (Figures 5b and 6b) commonly occur in the deepest part of the system within and immediately adjacent to the biotite tonalite and intermediate porphyry dikes. Potassic alteration is also characterized by veins containing quartz ± K-feldspar, biotite, epidote, anhydrite, magnetite, chalcopyrite (Type 3) (Figures 5c and 6c) and by patchy K-feldspar replacements within plagioclase phenocrysts. These veins have straight walls and commonly have a biotite halo,

variably replaced by chlorite. Locally, potassic alteration at Don Manuel can be texturally destructive, but primary textures of the intrusive units are commonly well preserved.

Sulfides associated with potassic alteration consist predominantly of chalcopyrite with lesser amounts of bornite, pyrite, and molybdenite. Vein-hosted sulfides and disseminates precipitated during this stage account for the highest-grade intervals and the majority of mineralization [13]. The potassic alteration and veins occur predominantly in the biotite tonalite and the intermediate porphyry dikes.

The potassic alteration progressively grades outward from the core of the system into propylitic alteration, predominantly in the adjacent wall rock. The dominant propylitic alteration mineral assemblage consists of chlorite, epidote, and actinolite with minor calcite. Chlorite is widespread in propylitic alteration of the Coya Machalí Formation, commonly along siltstone lithological layers. Chlorite ± actinolite replaces the primary mineral assemblages, including pyroxene, amphibole, and biotite, in basaltic andesite and intermediate porphyry dikes, destroying primary textures. Disseminated pyrite is common.

3.2. Primary Stage

Quartz ± K-feldspar, anhydrite, chalcopyrite, pyrite, bornite, specularite, molybdenite veins (Type 4) (Figure 5d,e and Figure 6d,e) are the earliest veins to host significant copper sulfides and define the primary mineralization stage. Quartz + K-feldspar ± anhydrite veins are common in the deeper part of the system (Figure 5d). The subdivision Type 4b veins consist of chalcopyrite ± quartz, pyrite and have sharp, straight vein walls most commonly without halos (up to 1 cm), but some have K-feldspar halos (Figures 5f and 6f). Type 4b veins can have well-developed, euhedral quartz crystals along the vein walls and chalcopyrite infilling the interior. These veins carry the bulk of the chalcopyrite in the Don Manuel porphyry copper system and are principally associated with the IPDs.

Also associated with the primary stage are veins containing chlorite + quartz ± actinolite, K-feldspar, pyrite, chalcopyrite which in some instances have halos of quartz (Type 5) (Figures 5g and 6g). Lastly, Type 6 veins host the majority of the molybdenite in the Don Manuel system. They contain quartz + anhydrite ± chalcopyrite, pyrite, molybdenite, bornite, specularite, anhydrite (Figure 5h). Types 5 and 6 veins are primarily hosted in the intermediate porphyry dikes, biotite tonalite and in the wall rocks of the Coya Machalí Formation adjacent to these two units. These veins are the latest in temporal development for the primary stage.

3.3. Late Stage

The late stage of alteration is the most texturally destructive, but it is very localized. This alteration is typically characterized by abundant chlorite and sericite, most often occurring as wide vein halos (up to 3 cm), which overprint pre-existing potassic alteration assemblages with chlorite replacing biotite and sericite replacing plagioclase and K-feldspar. Late-stage alteration is commonly developed near lithologic contacts, fractures, and within feldspar-rich volcaniclastic lithologies of the Coya Machalí Formation. In areas of sericite-chlorite alteration, plagioclase grains in the volcaniclastics have been entirely replaced by sericite. Additionally, the volcaniclastic groundmass has also been altered to sericite ± quartz. This alteration is focused along contacts or fractures and contains more pyrite than chalcopyrite. Veins of quartz ± chalcopyrite, pyrite, specularite, molybdenite, anhydrite, calcite veins (Types 7 and 8) have halos of sericite ± chlorite (Figures 5i–k and 6h). Specularite is common in veins associated with the chlorite-sericite alteration.

Advanced argillic alteration is uncommon and confined exclusively to narrow fractured zones with widths of less than 15 cm and to permeable layers within the wall rocks. Although sulfides are present, minerals such as gypsum, barite, anhydrite, carbonates (including ankerite and siderite), specularite, and clay minerals are more common. Tennantite-enargite, galena, sphalerite, pyrite, bournonite, and stibnite were observed locally in argillic alteration assemblages [13]. The tennantite-enargite occurs as rims replacing chalcopyrite in the Coya Machalí volcaniclastics. Type 9 veins consist of carbonate

(including calcite, ankerite and siderite) + barite, gypsum, specularite, pyrite, molybdenite with or without sericite halos (Figures 5l and 6i) and are associated with argillic alteration. Type 9 veins carry the only significant gold intercepts in the Don Manuel system. Gold occurs as 3–18 μm inclusions in pyrite [13].

3.4. Breccias

Breccias are much less common in the Don Manuel cores than in other porphyry copper deposits of the Miocene-Pliocene porphyry copper belt, where they typically host a significant portion of the copper sulfides [9–11,18–21]. At Don Manuel, hydrothermally cemented hornfels breccia, a hydrothermal polymict breccia, and an igneous breccia were recognized in the drill core.

Hornfels breccia intervals were identified in two drill holes and are less than 4 m thick. The quartz-anhydrite-cemented hornfels breccia (Figure 7a) is a monomict, clast supported with clasts of angular chlorite-altered mudstone (0.4 to >5 cm) and contains pyrite, but no chalcopyrite. A polymict, clast-supported breccia contains truncated chalcopyrite-quartz-pyrite veins within angular clasts of intermediate porphyry dike (IPD) adjacent to angular to sub-rounded clasts of propylitically altered mudstone hornfels and coarse sandstone (Figure 7b). Clasts range in size from 0.25 to >5 cm. A quartz-chalcopyrite-pyrite-specularite vein crosscuts the breccia. Calc-silicate breccia (Figure 7c) is clast supported and cemented by hydrothermal quartz and chlorite, with clasts ranging in size from 0.1 to 4 cm. The calc-silicate breccia contains conspicuous chalcopyrite mostly within the quartz cement and in veins that crosscut both the breccia clasts and intraclast void fill. It is part of a 16 m interval of >0.58% Cu [13]. The polymict matrix-supported igneous breccia has a net-veined texture and is weakly mineralized. Subangular clasts range in size from 0.3 to 10 cm and are mostly biotite tonalite and IPD, with minor basaltic andesite (Figure 7d,e). The matrix is of variably silicified IPD composition.

3.5. Hydrothermal Alteration at Paredones

Within the rhyolite stock, silicification has locally destroyed the original igneous texture and is associated with intense fracturing. Much of the Paredones area shows jarosite-goethite staining likely due to iron-bearing fluids circulating within the valley moraine. The staining is particularly prominent in the rhyolite stock and in travertine deposits around the moraine. At the northern valley wall in the Paredones area, intense argillic alteration is visible but inaccessible. However, boulders at the base of the slope contain veins and cavities with native sulfur, gypsum ± pyrite and clast-supported, hydrothermal breccias with clasts of porphyritic rock cemented by hydrothermal gypsum and iron oxide. No copper mineralization was observed in the Paredones area.

Figure 7. Breccia lithologies recognized in the Don Manuel system: hydrothermally cemented hornfels/calc-silicate breccia, polymict breccia, and igneous breccia. (**a**) Quartz-anhydrite-cemented hornfels breccia, DM6, 410 m. (**b**) Polymict breccia with clasts of IPD, mudstone hornfels and coarse sandstone, DM6, 419 m. (**c**) Calc-silicate breccia containing angular skarnoid clasts cemented together by quartz and chlorite, DM8, 597 m. (**d**) Igneous breccia with clasts of biotite tonalite, IPD, and basaltic andesite in an igneous matrix (melt) similar to the IPD. In this interval, the breccia shows additional silicification, DM4, 320. (**e**) An example of net-veined a version of the igneous breccia with visible clasts of basaltic andesite in an IPD-like matrix DM4, 563 m.

4. Methods

4.1. Re-Os Geochronology

The Re and Os contents in molybdenite from veins were measured by isotope dilution mass spectrometry at the University of Bristol, UK. Samples were handpicked under a

binocular microscope and then ground using an agate mortar and pestle. Samples were dissolved using a modified Carius tube technique based on the method of Shirey and Walker [22]. Molybdenite sample, ^{185}Re and ^{190}Os isotopic tracers, and inverse agua regia (3 mL HCl and 9 mL HNO_3) were added to the tubes which were then welded closed and placed in steel pipes in an oven for ~60 h at 230 °C to ensure sample dissolution and sample–spike equilibration.

Rhenium and Os were separated from the dissolved sample using solvent extraction techniques [23,24]. Osmium was separated using solvent extraction (hydrogen bromide and carbon tetrachloride) [24] and purified by microdistillation [23]. Rhenium was separated using solvent extraction (HNO_3 and 3-methyl-1-butanol [23]. The purified Re and Os samples were then loaded using 1 μL HBr onto Pt-filaments and isotopic compositions were measured by negative thermal ionization mass spectrometry (N-TIMS) with a Thermo Finnigan Triton. Isotopes were sequentially measured using a secondary electron multiplier. Total procedural blanks were 1.8 pg for Os and <5 pg for Re. Blank corrections have negligible effects on the calculated ^{187}Re and ^{187}Os concentrations. Deconvolution of the Os isotope data follows a similar method to that described in Markey et al. [25], but for a single rather than double spike. Uncertainties in the Os isotope data include correction for blank and uncertainties in the composition of the common Os. The uncertainty in the model age includes propagation of the uncertainties in the concentrations of ^{187}Re and ^{187}Os and the decay constant (1.666×10^{-11} a^{-1} with a 1% uncertainty). Two procedural blanks and one Henderson molybdenite standard (27.656 ± 0.022 Ma [26]) were also run with each of the Don Manuel molybdenite samples. Additional analytical methods and procedures are described in detail in Supplementary Material Method S1.

4.2. ^{40}Ar/^{39}Ar Geochronology

The ^{40}Ar/^{39}Ar method was used to date hydrothermal biotite from veins and ground-mass aggregate clots. Euhedral to subhedral hydrothermal biotite was separated from veins and zones of pervasive potassic alteration. The secondary biotite separated was distinguished from primary magmatic biotite based on its finer grain size, color, and texture. Unaltered biotite grains were handpicked under a binocular microscope. All samples were then cleaned in an ultrasonic bath with deionized water.

The sample package was irradiated in the Oregon State University reactor (Corvallis, Oregon; USA), Cd-shielded facility. Alder Creek sanidine (1.2056 Ma [27]) was used to monitor ^{39}Ar production and establish neutron flux values (J) for the samples. Gas was extracted from samples via step-heating using a mid-infrared (10.6 μm) CO_2 laser. Data were collected on a GVi instruments ARGUS V multicollector mass spectrometer using a variable-sensitivity Faraday collector array in static collection (non-peak hopping) mode [28,29]. Plateau acceptance criteria are at least four consecutive age steps that are indistinguishable at the 2σ level and represent 50% or more of the total ^{39}Ar released during the experiment. The scatter between these steps should be low (mean squared weighted deviation, MSWD approaching 1); for plateaus with excess scatter (MSWD > 95% CL), the uncertainty on the plateau age is multiplied by the square root of MSWD. Furthermore, the trapped component derived from an inverse isochron analysis should be indistinguishable from atmosphere. Additional analytical methods and procedures are described in detail in Supplementary Material Method S2. The inverse-variance weighted plateau ages represent the time at which the biotite cooled through the Ar closure temperature of ~350 °C [30].

5. Geochronology

The geochronological sequence for the intrusive units of the DMIC was previously established by Gilmer et al. [1] using CA-ID-TIMS U-Pb dating of zircons for the silicic units and the ^{40}Ar/^{39}Ar method on groundmass separates for the basaltic andesite dikes (Table 1). These dates agree with observed cross-cutting relationships and are interpreted as emplacement ages. Here, we report new Re-Os dates for sulfide mineralization and ^{40}Ar/^{39}Ar dates for hydrothermal alteration for samples collected from drill holes (Table 3).

Table 3. Sample locations and descriptions for ^{40}Ar/^{39}Ar and Re-Os geochronology.

Sample	Drill Hole, Depth (m), Elevation (m, a.s.l.)	Description	Mineral, Dating Technique
DM4AG13	DM4, 283, 2762	Porphyritic biotite tonalite with weak potassic alteration; Type 3 vein with quartz, biotite, potassium feldspar, and chalcopyrite	Biotite, ^{40}Ar/^{39}Ar
DM6AG22	DM6, 535, 2510	Intermediate porphyry dike (unclassified) with moderate potassic alteration; aggregate of secondary biotite associated with disseminated pyrite and chalcopyrite	Biotite, ^{40}Ar/^{39}Ar
DM2AG47	DM2, 358, 2722	Intermediate porphryry dike (unclassified) with intense potassic alteration; disseminated hydrothermal biotite	Biotite, ^{40}Ar/^{39}Ar
DM7AG40	DM7, 1049, 2263	Equigranular biotite tonalite with weak potassic alteration; Type 3 vein with quartz, biotite, fluorite, and chalcopyrite	Biotite, ^{40}Ar/^{39}Ar
DM5AG34	DM5, 503, 2737	Don Manuel Principal basaltic andesite dike crosscutting volcanic hornfels of the Coya Machali Formation	Whole rock, ^{40}Ar/^{39}Ar
DM5AG07	DM5, 146, 3094	Don Manuel Principal basaltic andesite dike crosscutting an intermediated porphyry dike	Whole rock, ^{40}Ar/^{39}Ar
DM8AG40	DM8, 546, 2620	Don Manuel Principal basaltic andesite dike crosscutting sedimentary hornfels of the Coya Machali Formation	Whole rock, ^{40}Ar/^{39}Ar
DM7AG06	DM7, 127, 3185	Don Manuel Principal basaltic andesite dike crosscutting sedimentary hornfels of the Coya Machali Formation	Whole rock, ^{40}Ar/^{39}Ar
DM4AG35	DM4, 564, 2481	Intermediate porphyry dike (IPD2) with weak potassic alteration; Type 6 vein quartz-anhydrite-molybdenite	Molybdenite, Re-Os
DM7AG31	DM7, 836, 2476	Silicified sedimentary hornfels of the Coya Machali Formation; Type 8 with quartz + molybdenite, chalcopyrite, anhydrite with a sericite halo	Molybdenite, Re-Os
DM7AG32	DM7, 839, 2473	Silicified sedimentary hornfels of the Coya Machali Formation; Type 8 with quartz + molybdenite, chalcopyrite, anhydrite with a sericite halo	Molybdenite, Re-Os

5.1. Molybdenite Re-Os Geochronology

Three molybdenite samples from Types 6 and 8 veins (Supplementary Material Figure S1) were dated using the Re-Os geochronological method. Sample descriptions and locations are presented in Table 3. Re-Os molybdenite ages and Re and Os concentrations are presented in Table 4. Uncertainties on the ages incorporate propagation of uncertainties from the decay constant for ^{187}Re ($1.666 \times 10^{-11} \pm 0.017$ yr^{-1}), taken from Smoliar et al. [31], the blank correction, the oxygen isotope composition of the oxygen that forms the negative ions in the mass spectrometer and the estimated range of ^{187}Os/^{188}Os in the common Os correction estimated from Mathur et al. [32]. Two of the three molybdenite samples, DM7AG31 and DM7AG32, had Re concentrations of 204.7 and 127.8 ppm, respectively. They yielded ages of 3.416 ± 0.037 and 3.425 ± 0.037 Ma. A third sample, DM4AG35, had significantly less Re, 95.7 ppm, and yielded a much younger age of 0.814 ± 0.009 Ma.

Table 4. Re-Os data for Don Manuel molybdenite.

Sample	wt (g)	Re (ppm)	2σ	^{187}Re (ppm)	2σ	^{187}Os (ppb)	2σ	Date (Ma)	2σ
DM4AG35	0.049	95.72	0.27	60.16	0.17	0.82	0.002	0.814	0.009
DM7AG31	0.050	204.73	0.37	128.68	0.23	7.32	0.02	3.416	0.037
DM7AG32	0.047	127.76	0.13	80.31	0.08	4.58	0.02	3.425	0.037

5.2. Hydrothermal Biotite ^{40}Ar/^{39}Ar Geochronology

Sample descriptions, locations, and images are presented in Table 3 and Supplementary Material Figure S2. Biotite ^{40}Ar/^{39}Ar plateau dates and isochrons are presented in Figure 8 and Supplementary Material Table S1. Biotite from sample DM4AG13, a Type 3 vein containing biotite, potassium feldspar, quartz, and chalcopyrite from the porphyritic phase of the biotite tonalite yielded a seven-step plateau date of 3.57 ± 0.02 Ma (MSWD = 0.84). The inverse isochron date of 3.55 ± 0.05 Ma is concordant with an ^{40}Ar/^{36}Ar ratio of 314 ± 18 (Figure 8a). Sample DM6AG22 is a clot of secondary biotite associated with disseminated pyrite and chalcopyrite from the intermediate porphyry

and yielded a ten-step plateau date of 3.51 ± 0.02 Ma (MSWD = 1.16). The inverse isochron date of 3.48 ± 0.07 Ma is concordant with an ^{40}Ar/^{36}Ar ratio of 309.6 ± 9.2 (Figure 8b). Disseminated biotite from sample DM2AG47 from a zone of intense potassic alteration within the hybridized intermediate porphyry yielded an eight-step plateau date of 3.41 ± 0.01 Ma (MSWD = 0.49). The inverse isochron age of 3.41 ± 0.06 Ma is concordant with an ^{40}Ar/^{36}Ar ratio of 297.8 ± 2.0 (Figure 8c). A Type 3 vein containing sample DM7AG40 biotite, anhydrite, quartz, and chalcopyrite from the equigranular phase of the biotite tonalite yielded a seven-step plateau age of 3.37 ± 0.01 Ma (MSWD = 1.35). The inverse isochron date of 3.36 ± 0.09 Ma is concordant with an ^{40}Ar/^{36}Ar ratio of 304.4 ± 4.6 (Figure 8d).
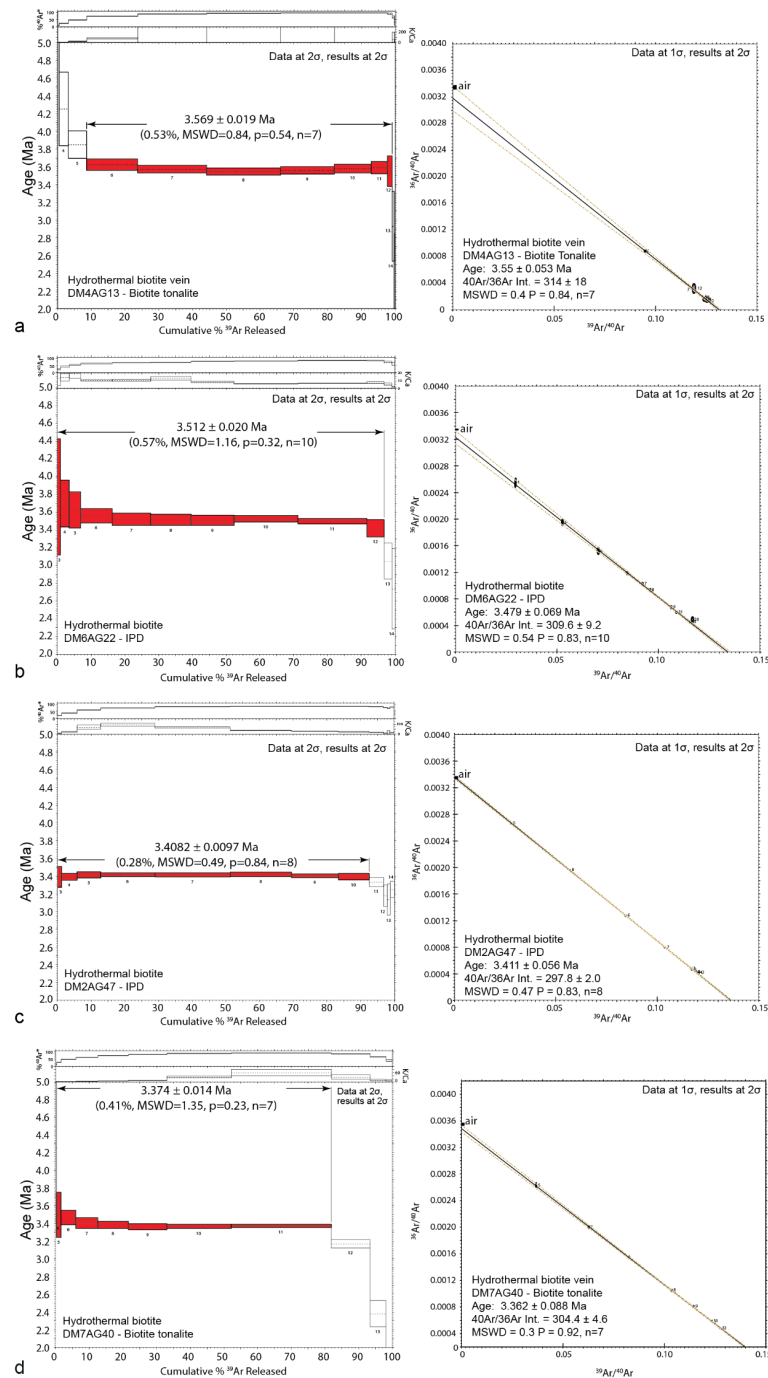
Figure 8. Hydrothermal biotite ^{40}Ar/^{39}Ar plateau (shown in red) and inverse isochron ages for (**a**) Sample DM6AG22. (**b**) Sample DM2AG47. (**c**) Sample DM4AG13. (**d**) Sample DM7AG40. All uncertainties are shown at the 2σ confidence level.

From the inverse isochron analysis, two samples, DM6AG22 and DM7AG40, have trapped $^{40}Ar/^{36}Ar$ compositions that are slightly enriched in ^{40}Ar relative to atmosphere, indicating an excess argon component may be present in the biotites. However, recalculating the apparent ages and accounting for this excess component yields ages that are at most 10–30 k.y. younger, but indistinguishable at 2σ from the original age calculation (listed in Supplementary Material Table S1), and so we take the original calculation as the best estimate of the cooling age.

All of the hydrothermal biotite $^{40}Ar/^{39}Ar$ ages are younger than the youngest intrusion ages by ~300 k.y. (Figure 9). While the zircon ages record emplacement ages of the intrusive units biotite ages record the time at which the rocks cooled to temperatures below the blocking temperature of approximately 350 °C [30]. Taken together, the age differences provide constraints on the thermal history of DMIC.
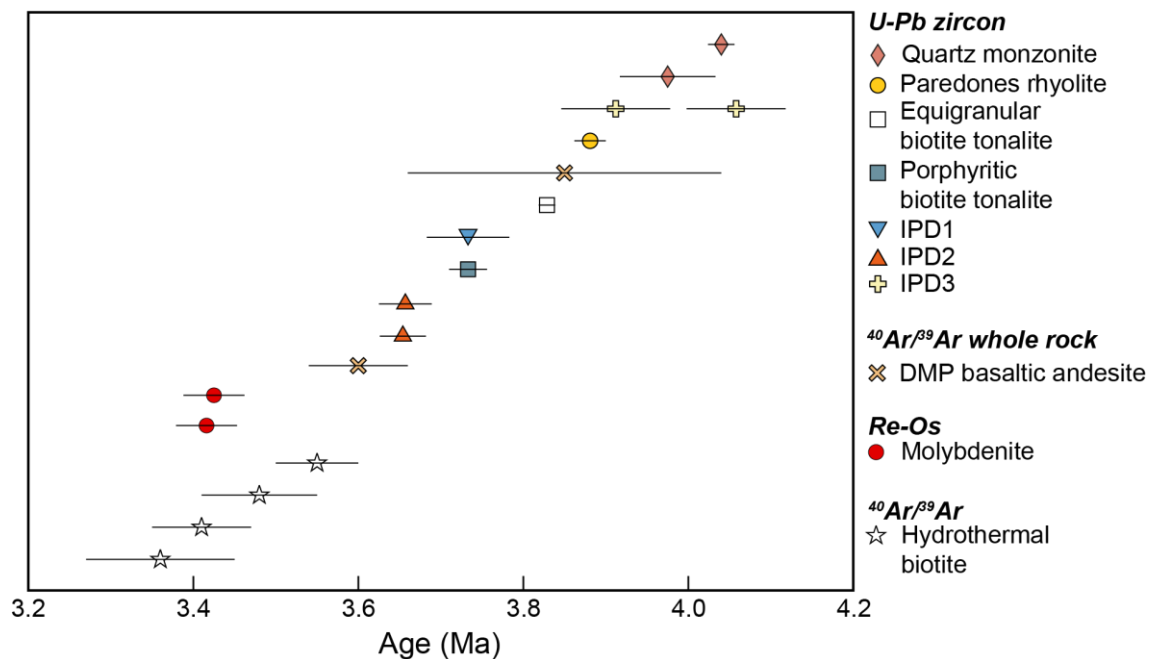

Figure 9. Summary of radiogenic ages for the igneous intrusions of the DMIC, mineralization, and hydrothermal alteration. U-Pb zircon ages and whole rock $^{40}Ar/^{39}Ar$ ages from Gilmer et al. [1].

6. Discussion

The Don Manuel porphyry copper system contains many features typical of porphyry copper deposits worldwide including (1) multiple intrusive pulses; (2) potassic alteration associated with the majority of copper mineralization; (3) subsequent discontinuous and vein-related chlorite-sericite and sericite alteration; (4) potassic alteration (albeit discontinuous) surrounded by propylitic alteration, especially within the wall rock lithologies; (5) localized lithologically controlled skarn development; and (6) structurally controlled argillic alteration. Notwithstanding the limited surface exposures and drill holes, a sequence can be recognized. The alteration and mineralization can be divided into silicification and calc-silicate alteration, early stage, primary, and late stages.

The Don Manuel igneous complex and porphyry system began with the emplacement of the ca. 4.04 Ma quartz monzonite in the Don Manuel Principal area and the ca. 3.88 Ma rhyolite in the Paredones area into the volcanic and sedimentary country rocks of the Coya Machalí Formation. In the Don Manuel Principal area, alteration of the country rock is attributed to the emplacement of biotite tonalite and various pulses of IPD. These represent early and synmineralization intrusive activity and are associated with potassic and magnetite alteration. Most of the sulfide mineralization occurred during this stage. The two older Re-Os dates for vein-hosted molybdenite fall within the range of dates for

hydrothermal alteration of DMIC (Figure 9). However, we cannot tie the Re-Os dates to specific intrusive units. The one younger Re-Os date on molybdenite could be unrelated to the Pliocene mineralization or may represent post-mineralization alteration. Although there was no observable indication of such alteration in this vein (see Supplementary Material Figure S1), McCandless et al. [33] found that Re loss can occur in both the hypogene and supergene environments due to advecting fluids, resulting in ages which are too young. Additional microscopy (e.g., infrared, electron probe microanalysis, X-ray diffraction, backscattered electron imaging) is necessary to evaluate this possibility.

Potassic alteration is the dominant type and suggests a lack of acidity in the hydrothermal fluids circulating during the lifetime of the Don Manuel system. Texturally destructive hydrolytic alteration (chlorite-sericite and sericite) is limited to late-stage vein selvages, fractures, and contact margins in the Don Manuel system. Cooling and decrease in pressure likely increase the acidity in the system explaining this transition [34–37]. Sericitic alteration may have developed contemporaneously with potassic alteration at a shallower level but has subsequently been eroded, though observations recorded in this study indicate that, at least at deeper levels in the system, sericitic alteration postdated and overprinted potassic alteration. The lowest temperature alteration and veins include carbonate-specularite veins and carbonate-clay assemblages, which are also structurally controlled.

Groundmass $^{40}Ar/^{39}Ar$ dates (ca. 3.85 and 3.60 Ma) for the basaltic andesite dikes indicate that they intruded periodically throughout the emplacement of the DMIC. Some dikes, with hydrothermal actinolite and chlorite partially replacing primary amphibole, likely intruded towards the waning of the DMIC system. These late-mineralization dikes contain pyrite veinlets and rarely chalcopyrite-quartz veinlets. Also, post-mineralization basaltic andesite dikes are unaltered.

6.1. Lifespan of the Hydrothermal System

The Don Manuel hydrothermal system cooled variably as recorded by the hydrothermal biotite cooling ages, with the deepest sample recording the youngest age (Table 3 and Figure 8) as the isotherms retracted downward with time. The $^{40}Ar/^{39}Ar$ hydrothermal biotite ages show that the timing of hydrothermal alteration in the Don Manuel system continued for at least ~300 k.y. after the main intrusions were emplaced (Figure 9). The closure temperature for biotite is ~350 °C [30]; thus, these data constrain the cooling through the closure temperature in each of the samples with the deepest sample being the youngest. Suzuki et al. [38] suggested that the closure temperature for the Re-Os system in molybdenite is ~500 °C based on comparisons with Rb-Sr ages from ore deposits in Japan. Combining the Re-Os molybdenite age data and the $^{40}Ar/^{39}Ar$ hydrothermal biotite cooling ages with the U-Pb zircon ages presented in Gilmer et al. [1] shows that hydrothermal activity in this system lasted at least 600 k.y.

Models of active magmatic volatile fluxing associated with mineralization [39,40] show that temperatures well above the blocking temperature of biotite and molybdenite (i.e., >500 °C) can be maintained in the shallow crust above a magmatic system at depths of 3.5 to 5 km. However, cooling through a combination of conductive heat loss and extraction of heat from the overlying convective hydrothermal meteoric system will occur. Time scales for cooling below the blocking temperatures are only on the order of a few tens of thousands of years (see Figure 7 in Weis [39] Figure 8 in Afanasyev et al. [40]). Thus, the observation that the ages of biotite and molybdenite are a few hundred thousands of years younger than the association high-level intrusions suggests that the deeper magmatic system continued to be active and supply high-temperature mineralizing fluids long after shallow magma intrusion.

6.2. Comparisons with Other Miocene–Pliocene Deposits in Central Chile

The portions of the Don Manuel porphyry copper system that have been drilled or exposed lack several characteristics associated with the giant PCDs of the Miocene-Pliocene porphyry copper belt of central Chile which are aligned north–south in the

Western Cordillera. For example, the El Teniente, Los Bronces-Río Blanco, and Los Pelambres deposits all contain extensive magmatic and hydrothermal brecciation that hosts significant copper sulfide mineralization, as well as other breccia units that postdate mineralization [2,9,41–43]. At Los Bronces-Río Blanco, ten separate breccia types have been defined and approximately half of the copper sulfide mineralization is hosted by breccia [2,10]. Each of the felsic to intermediate porphyry emplacement phases at El Teniente is interpreted to have had an associated brecciation event [21]. Extensive brecciation creates permeability and focuses fluid flow. Don Manuel, by contrast, contains comparably little breccia, and the breccias present do not contain significant copper sulfides. The DMIC may have been emplaced too deep (3.5 to 5 km [14]) to have experienced the necessary deviations from lithostatic pressure to generate vertically extensive breccias. Much more pervasive hydrothermal alteration and, in particular, more extensive sericitic alteration are also present in each of the other giant PCDs of the Miocene–Pliocene belt compared with that of Don Manuel.

With only eight holes drilled at Don Manuel Principal, the extent of the resource is not fully defined and additional drilling could extend the resource and potentially reveal additional localized alteration and brecciation. It is also possible that brecciation and significant sericitic alteration existed in the system but have been removed by erosion. Alternatively, the Don Manuel system may just be a much smaller system driven by exsolved fluids from a smaller magma reservoir in the shallow crust.

6.3. Uplift and Exhumation of the DMIC and Porphyry Copper System

In the ~4–3.6 M.y. since their emplacement, the DMIC units now exposed at the surface have been exhumed from a depth of 3.5–5 km, corresponding to an average exhumation rate of 1.0–1.4 km/M.y. Rapid exhumation has implications for the preservation potential of similar-aged or older hypogene ore deposits in this part of the eastern Principal Cordillera. The proportion of the Don Manuel porphyry copper system missing due to erosion is not known. The DMIC, though largely covered at the surface, does crop out in both the Don Manuel Principal area and the Paredones area. A considerable volume of rock could have been lost to erosion and with it valuable mineralization. The predominance of potassic alteration over other types of alteration suggests that the majority of the accessible system (i.e., drill core) represents the deeper levels of the hydrothermal system (e.g., [36]) supporting the possibility that much of the system has been eroded away.

Alternatively, if the Don Manuel system is a highly telescoped system, albeit with the majority of the upper portion of the system having been removed by erosion, then mineralization may have expanded vertically. Despite the lack of known stockwork veining, it is possible that additional resources may yet be encountered at depth. Recent work documenting root zones of porphyry copper systems [44,45] show that these deeper parts of the system are cored by potassic alteration. However, this system lacks other features observed in the root zones of other PCDs, namely coarse-grained muscovite [44]. Although bornite was observed in the drill core, it is rare; a true central bornite-chalcopyrite zone, often present in porphyry copper deposits and present in all known economic Miocene–Pliocene systems, was not encountered in the core at Don Manuel, leaving open the possibility that this zone may not have been reached by drilling. If uplift rates have remained high over that last few million years, then there is potential for undiscovered, highly telescoped systems closer to the active arc.

7. Conclusions

The hydrothermal alteration recognized at Don Manuel consists of early silicification and calc-silicate alteration, sodic-calcic alteration, potassic alteration, propylitic alteration, sericite-chlorite alteration and argillic alteration. Hydrothermal biotite ages are younger than the youngest intrusion by ~300 k.y. recording the cooling of the system below 350 °C. Re-Os molybdenite ages are consistent with the hydrothermal biotite ages. Models of magmatic fluid fluxing [39,40] indicate that a deeper magmatic system must have been

active after shallow magma intrusion had ceased. Although Don Manuel displays many of the features common to other porphyry systems in the Miocene–Pliocene metallogenic belt, it is a smaller resource and lacks significant brecciation and sericitic alteration. However, much of the system could still underlie what has been described at Don Manuel, leaving open the possibility of additional resources at depth.

References

1. Gilmer, A.K.; Sparks, S.; Rust, A.C.; Tapster, S.; Webb, A.D.; Barfod, D.N. Geology of the Don Manuel igneous complex, central Chile: Implications for igneous processes in porphyry copper systems. *GSA Bull.* **2017**, *129*, 920–946. [CrossRef]
2. Skewes, M.A.; Stern, C.R. Tectonic trigger for the formation of late Miocene Cu-rich breccia pipes in the Andes of central Chile. *Geology* **1994**, *22*, 551. [CrossRef]
3. Kay, S.M.; Godoy, E.; Kurtz, A. Episodic arc migration, crustal thickening, subduction erosion, and magmatism in the south-central Andes. *GSA Bull.* **2005**, *117*, 67. [CrossRef]
4. Marot, M.; Monfret, T.; Gerbault, M.; Nolet, G.; Ranalli, G.; Pardo, M. Flat versus normal subduction zones: A comparison based on 3-D regional traveltime tomography and petrological modelling of central Chile and western Argentina (29°–35°S). *Geophys. J. Int.* **2014**, *199*, 1633–1654. [CrossRef]
5. Farías, M.; Comte, D.; Charrier, R.; Martinod, J.; David, C.; Tassara, A.; Tapia, F.; Fock, A. Crustal-scale structural architecture in central Chile based on seismicity and surface geology: Implications for Andean mountain building. *Tectonics* **2010**, *29*, 29. [CrossRef]
6. Yáñez, G.; Cembrano, J.; Pardo, M.; Ranero, C.; Selles, D. The Challenger–Juan Fernández–Maipo major tectonic transition of the Nazca–Andean subduction system at 33–34 S: Geodynamic evidence and implications. *J. S. Am. Earth Sci.* **2002**, *15*, 23–38. [CrossRef]
7. Stern, C.R. Active Andean volcanism: Its geologic and tectonic setting. *Rev. Geol. Chile* **2004**, *31*, 161–206. [CrossRef]
8. Pardo, M.; Comte, D.; Monfret, T. Seismotectonic and stress distribution in the central Chile subduction zone. *J. S. Am. Earth Sci.* **2002**, *15*, 11–22. [CrossRef]
9. Cannell, J.; Cooke, D.R.; Walshe, J.L.; Stein, H. Geology, Mineralization, Alteration, and Structural Evolution of the El Teniente Porphyry Cu-Mo Deposit. *Econ. Geol.* **2005**, *100*, 979–1003. [CrossRef]
10. Warnaars, F.W.; Holmgren, D.C.; Barassi, F.S. Porphyry copper and tourmaline breccias at Los Bronces-Rio Blanco, Chile. *Econ. Geol.* **1985**, *80*, 1544–1565. [CrossRef]
11. Davidson, P.; Kamenetsky, V.S.; Cooke, D.R.; Frikken, P.; Hollings, P.; Ryan, C.G.; Van Achterbergh, E.; Mernagh, T.; Skarmeta, J.; Serrano, L.; et al. Magmatic Precursors of Hydrothermal Fluids at the Rio Blanco Cu-Mo Deposit, Chile: Links to Silicate Magmas and Metal Transport. *Econ. Geol.* **2005**, *100*, 963–978. [CrossRef]

12. Maksaev, V.; Townley, B.; Palacios, C.; Camus, F. Metallic ore deposits. In *The Geology of Chile*; Geological Society of London: London, UK, 2018; pp. 179–199.

13. Candia, W.; Oviedo, O.; Nuñez, E. Don Manuel Project Seasonal Report. In *Minera Aurex Reports*; Minera Aurex: Santiago, Chile, 2009; p. 52.

14. Gilmer, A.K.; Sparks, R.S.J.; Blundy, J.D.; Rust, A.; Hauff, F.; Hoernle, K.; Spencer, C.J.; Tapster, S.; Stephen, R.; Sparks, J. Petrogenesis and Assembly of the Don Manuel Igneous Complex, Miocene–Pliocene Porphyry Copper Belt, Central Chile. *J. Pet.* **2018**, *59*, 1067–1108. [CrossRef]

15. Charrier, R.; Wyss, A.; Flynn, J.J.; Swisher, C.C., III; Norell, M.A.; Zapatta, F.; McKenna, M.C.; Novacek, M.J. New evidence for late Mesozoic-early Cenozoic evolution of the Chilean Andes in the upper Tinguiririca valley (35 S), central Chile. *J. S. Am. Earth Sci.* **1996**, *9*, 393–422. [CrossRef]

16. Charrier, R.; Baeza, O.; Elgueta, S.; Flynn, J.; Gans, P.; Kay, S.; Muñoz, N.; Wyss, A.; Zurita, E. Evidence for Cenozoic extensional basin development and tectonic inversion south of the flat-slab segment, southern Central Andes, Chile (33°–36° S.L.). *J. S. Am. Earth Sci.* **2002**, *15*, 117–139. [CrossRef]

17. Godoy, E.; Yañez, G.; Vera, E. Inversion of an Oligocene volcano-tectonic basin and uplifting of its superimposed Miocene magmatic arc in the Chilean Central Andes: First seismic and gravity evidences. *Tectonophysics* **1999**, *306*, 217–236. [CrossRef]

18. Atkinson, W.W., Jr.; Souviron, A.; Vehrs, T.I.; Faunes, A. Geology and Mineral Zoning of the Los Pelambres Porphyry Copper Deposit. *Soc. Econ. Geol. Spec. Publ.* **1996**, *5*, 131–156.

19. Spencer, E.T.; Wilkinson, J.J.; Creaser, R.A.; Seguel, J. The Distribution and Timing of Molybdenite Mineralization at the El Teniente Cu-Mo Porphyry Deposit, Chile. *Econ. Geol.* **2015**, *110*, 387–421. [CrossRef]

20. Bertens, A.; Clark, A.; Barra, F.; Deckart, K. Evolution of the Los Pelambres-El Pachón porphyry copper-molybdenum district, Chile/Argentina. In Proceedings of the XI Congreso Geológico Chileno, Short Papers, Antofagasta, Chile, 7–11 August 2006; pp. 179–181.

21. Vry, V.H.; Wilkinson, J.; Seguel, J.; Millán, J. Multistage Intrusion, Brecciation, and Veining at El Teniente, Chile: Evolution of a Nested Porphyry System. *Econ. Geol.* **2010**, *105*, 119–153. [CrossRef]

22. Shirey, S.B.; Walker, R.J. Carius Tube Digestion for Low-Blank Rhenium-Osmium Analysis. *Anal. Chem.* **1995**, *67*, 2136–2141. [CrossRef]

23. Birck, J.-L.; Barman, M.R.; Capmas, F. Re-Os Isotopic Measurements at the Femtomole Level in Natural Samples. *Geostand. Geoanal. Res.* **1997**, *21*, 19–27. [CrossRef]

24. Cohen, A.S.; Waters, F. Separation of osmium from geological materials by solvent extraction for analysis by thermal ionisation mass spectrometry. *Anal. Chim. Acta* **1996**, *332*, 269–275. [CrossRef]

25. Markey, R.; Hannah, J.L.; Morgan, J.W.; Stein, H.J. A double spike for osmium analysis of highly radiogenic samples. *Chem. Geol.* **2003**, *200*, 395–406. [CrossRef]

26. Markey, R.; Stein, H.; Hannah, J.L.; Zimmerman, A.; Selby, D.; Creaser, R.A. Standardizing Re–Os geochronology: A new molybdenite Reference Material (Henderson, USA) and the stoichiometry of Os salts. *Chem. Geol.* **2007**, *244*, 74–87. [CrossRef]

27. Renne, P.R.; Mundil, R.; Balco, G.; Min, K.; Ludwig, K.R. Joint determination of 40K decay constants and 40Ar∗/40K for the Fish Canyon sanidine standard, and improved accuracy for 40Ar/39Ar geochronology. *Geochim. Cosmochim. Acta* **2010**, *74*, 5349–5367. [CrossRef]

28. Mark, D.F.; Barfod, D.; Stuart, F.M.; Imlach, J. The ARGUS multicollector noble gas mass spectrometer: Performance for40Ar/39Ar geochronology. *Geochem. Geophys. Geosyst.* **2009**, *10*, 10. [CrossRef]

29. Sparks, R.S.J.; Folkes, C.B.; Humphreys, M.C.; Barfod, D.N.; Clavero, J.; Sunagua, M.C.; McNutt, S.R.; Pritchard, M.E. Uturuncu volcano, Bolivia: Volcanic unrest due to mid-crustal magma intrusion. *Am. J. Sci.* **2008**, *308*, 727–769. [CrossRef]

30. Grove, M.; Harrison, T.M. 40Ar* diffusion in Fe-rich biotite. *Am. Mineral.* **1996**, *81*, 940–951. [CrossRef]

31. Smoliar, M.I.; Walker, R.J.; Morgan, J.W. Re-Os Ages of Group IIA, IIIA, IVA, and IVB Iron Meteorites. *Science* **1996**, *271*, 1099–1102. [CrossRef]

32. Mathur, R.; Ruiz, J.; Munizaga, F. Relationship between copper tonnage of Chilean base-metal porphyry deposits and Os isotope ratios. *Geology* **2000**, *28*, 555–558. [CrossRef]

33. McCandless, T.E.; Ruiz, J.; Campbell, A.R. Rhenium behavior in molybdenite in hypogene and near-surface environments: Implications for Re-Os geochronometry. *Geochim. Cosmochim. Acta* **1993**, *57*, 889–905. [CrossRef]

34. Fournier, R.O. Hydrothermal processes related to movement of fluid from plastic into brittle rock in the magmatic-epithermal environment. *Econ. Geol.* **1999**, *94*, 1193–1211. [CrossRef]

35. John, D.; Ayuso, R.; Barton, M.; Blakely, R.; Bodnar, R.; Dilles, J.; Gray, F.; Graybeal, F.; Mars, J.; Mc Phee, D. *Porphyry Copper Deposit Model, Chap. B of Mineral Deposit Models for Resource Assessment*; US Geological Survey Scientific Investigations Report 2010-5070-B; USGS: Denver, CO, USA, 2010.

36. Sillitoe, R.H. Porphyry Copper Systems. *Econ. Geol.* **2010**, *105*, 3–41. [CrossRef]

37. Giggenbach, W.F. The origin and evolution of fluids in magmatic-hydrothermal systems. In *Geochemistry of Hydrothermal Ore Deposits*, 3rd ed.; Barnes, H.L., Ed.; John Wiley & Sons: New York, NY, USA, 1997; pp. 737–796.

38. Suzuki, Y.; Ioka, S.; Muraoka, H. Determining the Maximum Depth of Hydrothermal Circulation Using Geothermal Mapping and Seismicity to Delineate the Depth to Brittle-Plastic Transition in Northern Honshu, Japan. *Energies* **2014**, *7*, 3503–3511. [CrossRef]

39. Weis, P. The dynamic interplay between saline fluid flow and rock permeability in magmatic-hydrothermal systems. *Geofluids* **2015**, *15*, 350–371. [CrossRef]
40. Afanasyev, A.A.; Blundy, J.; Melnik, O.; Sparks, S. Formation of magmatic brine lenses via focussed fluid-flow beneath volcanoes. *Earth Planet. Sci. Lett.* **2018**, *486*, 119–128. [CrossRef]
41. Deckart, K.; Clark, A.H.; Celso, A.A.; Ricardo, V.R.; Bertens, A.N.; Mortensen, J.K.; Fanning, C.M. Magmatic and Hydrothermal Chronology of the Giant Rio Blanco Porphyry Copper Deposit, Central Chile: Implications of an Integrated U-Pb and 40Ar/39Ar Database. *Econ. Geol.* **2005**, *100*, 905–934. [CrossRef]
42. Reich, M.; Parada, M.A.; Palacios, C.; Dietrich, A.; Schultz, F.; Lehmann, B. Adakite-like signature of Late Miocene intrusions at the Los Pelambres giant porphyry copper deposit in the Andes of central Chile: Metallogenic implications. *Miner. Depos.* **2003**, *38*, 876–885. [CrossRef]
43. Stern, C.R.; Skewes, M.A. Miocene to present magmatic evolution at the northern end of the Andean Southern Volcanic Zone, Central Chile. *Andean Geol.* **1995**, *22*, 261–272.
44. Runyon, S.E.; Seedorff, E.; Barton, M.D.; Steele-MacInnis, M.; Lecumberri-Sanchez, P.; Mazdab, F.K. Coarse muscovite veins and alteration in porphyry systems. *Ore Geol. Rev.* **2019**, *113*, 103045. [CrossRef]
45. Seedorff, E.; Barton, M.D.; Stavast, W.J.A.; Maher, D.J. Root Zones of Porphyry Systems: Extending the Porphyry Model to Depth. *Econ. Geol.* **2008**, *103*, 939–956. [CrossRef]